Highlights

Modeling Hydraulic and Structural Serviceability Hazards of Reinforced Concrete Culverts

Mearg Ngusse SAHLE,Zachery Taylor HOWELL

- Developed a dual hazard framework for reinforced concrete culverts
- Compared six survival models on 2190 culverts using AIC and log likelihood criteria
- Gamma frailty Cox model best captured unobserved heterogeneity in hazard rates
- Results demonstrate hydraulic hazards emerge earlier, whereas structural hazards accumulate steadily
- Reported culvert-level hazard rates for both hydraulic and structural risks

Modeling Hydraulic and Structural Serviceability Hazards of Reinforced Concrete Culverts

Mearg Ngusse SAHLE[a,*,1], Zachery Taylor HOWELL[b,2]

[a]*Dept. of Global Engineering, Osaka University, 1-1 Yamadaoka, Suita, 565-0871, Osaka, Japan*
[b]*De San Nicholas Logistics, 18501 Ambly LN, Tampa, FL, 33647, U.S.A.*

ARTICLE INFO

Keywords:
reinforced concrete culverts
serviceability hazard
hydraulic inadequacy
structural weakness
Cox proportional hazards
gamma frailty

ABSTRACT

This paper presents a data-driven dual-hazard framework for estimating hydraulic and structural serviceability hazard rates in reinforced concrete culverts, which serve both traffic support and water conveyance functions. A network-level dataset of 2,190 reinforced concrete culverts in Ethiopia was used to model two types of serviceability hazards. Hydraulic hazards, driven by sedimentation, overtopping, and scouring, were modeled as functions of discharge depth, barrel slope, and barrel length. Structural hazards, resulting from fatigue cracking and chemical degradation, were modeled using average daily truck traffic, soil pH, and soil salinity. To identify the best-fitting model, six survival models were compared using Akaike Information Criterion, log-likelihood, and residual diagnostics. The Γ-frailty Cox proportional hazards model provided the best fit for both scenarios and effectively captured unobserved heterogeneity. Hydraulic risk decreased significantly with steeper barrel slopes, while discharge depth and barrel length had no significant effects. Structural risk increased with higher $ADTT$ and was mitigated by more alkaline soils. Soil salinity was excluded due to violations of model assumptions. Hazard rate distributions showed greater variability in hydraulic risk across the network, while structural risk was relatively uniform with isolated extremes. Hydraulic failure tended to occur earlier in the lifecycle, particularly in flatter and longer culverts. Structural deterioration was driven by traffic-induced fatigue and moderated by soil alkalinity. Covariate-stratified survival curves and relative hazard distributions identified critical subpopulations for targeted inspection. This framework supports optimized maintenance planning by prioritizing hydraulic assessments for flat, long culverts and structural evaluations for high-traffic, acidic sites.

1. Introduction

Reinforced concrete culvert structures are designed with a certain life expectancy, design life, to withstand estimated operating environmental, geographic, geological, and traffic loading conditions. Legitimately, their structural performance is measured in terms of limit states that satisfy the strength, safety, and serviceability requirements for the estimated load combinations.

** Corresponding author
m.sahle@civil.eng.osaka-u.ac.jp (M.N. SAHLE)
ORCID(s): 0000-0009-0003-7576-5518 (M.N. SAHLE)
[1]Graduate Student, Dept. of Global Engineering, Osaka University, Osaka, Japan.
[2]Independent Researcher, De San Nicholas Logistics, Tampa, Florida, U.S.A.

If the actual conditions are commensurate with the estimated design parameters; then the service life would not be less than the design life, excluding cases of failure due to extreme weather events, defective design, or substandard construction. During the operation phase of the structures, periodic inspection and maintenance are performed to extend service life and prevent premature failure. Figure 1 illustrates the trade-off between design life and service life in terms of cost, showing that while design and construction costs increase with longer service lives, operation and maintenance costs initially decrease, resulting in a minimum total life cycle cost at the optimal economic life.

The design process therefore sets the expected level of performance against the cumulative long-term effect of the operating conditions, and the possible inducements of sedimentation, erosion, flooding, and/ or material degradation failure modes. Culverts are designed primarily hydraulically except where difficult geometry dictates otherwise [1]. The hydraulic design of the culverts sets the minimum parameters to ensure the protection of roads through the prevention of water damage.

The hydraulic control of culverts could be at the outlet or inlet, depending on the direction at which the flow is passing through the critical depth. The type of control is designed by adopting the greater of the headwater depths calculated for both scenarios [1]. Culverts built on flatter terrains having less concentrated, poorly defined, spread flow are outlet controlled. Since the control point is at the outlet or downstream in the tailwater; the culvert is subject to head-losses at the entrance, invert, and exit. Thus, the inlet configuration, barrel characteristics (roughness, area, shape, length, slope), and the tailwater elevation affect performance of the culvert. In contrast, inlet control culverts are typically built on steeper slopes. Since the control is at the upstream end of the culvert, only the headwater and the inlet configuration affect the culvert performance. Depending on the tailwater condition, energy is dissipated through a hydraulic jump that occurs downstream of the inlet (i.e., unsubmerged outlet) or preferably in the culvert barrel (i.e., submerged outlet).

In outlet-controlled culverts, flow velocities are widespread and/or shallow. Thus, conditions downstream of the culvert can significantly affect the flow rate [2]. Consequently, minor downstream obstructions or land use alterations can divert the flow, affecting a considerable upstream channel segment. Thus, a sudden change in stream geometry or gradient that reduces stream

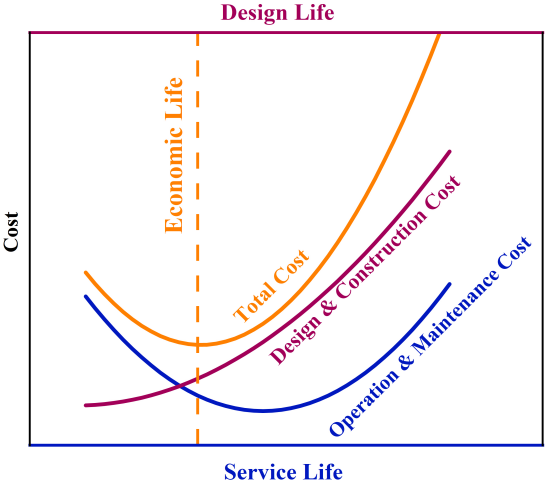

Figure 1: Design decisions of infrastructure life cycle expenditure.

velocity results in sediment aggradation and debris accumulation in the flow path, which in turn decreases the flow capacity, eventually instigating overtopping of banks.

However, inlet-controlled culverts are prone to erosion due to turbulence at the outlet or invert caused by high flow velocities that may arise when downstream water levels are low [2]. Erosion upsets the ability of culverts to direct flow. Damage of culvert invert also causes piping/ internal erosion of the supporting soil beneath these buried structures which gives rise to a differential settlement that induces displacement, cracking, or a total collapse at the worst.

In general, culvert performance is governed by watercourse geometry and gradient. Thus, any alteration of the prior channel characteristics affecting the designed flow parameters such as velocity, depth of flow, and energy, results in erosion, sedimentation, or flooding. Channel alignment has a significant influence on flow velocity, and velocity in turn has a significant effect on sediment transport and scour potential [1]. The natural channel geometry dictates the size and configuration of culverts, contingent up on the magnitude of flow velocities and afflux. Thus, the vertical alignment of pavement is adjusted considering allowable headwater levels, afflux, and minimum cover requirements. Generally, flooding arises when afflux exceeds culvert flow conveyance capacity due to flow constriction, heavy storm surge or rain, or higher downstream water level (i.e., lower slope in upstream). Flood-induced embankment saturation accelerates bank slumping, erosion, and washing.

The other mode of culvert failure is load or environment induced barrel material degradation. The degradation of reinforced concrete material is usually manifested through crack propagation leading to delamination/ spalling of concrete (i.e., excluding plastic cracks), followed by corrosion of reinforcing steel bars. These cracks could be initiated due to soil pressure / settlement, and fatigue stress from traffic loading. The dynamic load-induced deterioration of reinforced concrete culverts is highly dependent on the axle load exceeding the fatigue limit state. The fatigue limit state is the stress range where stress under repetitive cycles of design truck load is limited to prevent crack growth and fracture during the design life of a culvert [2]. Mechanical and chemical variables in the environment such as freeze-thaw cycles, alkali-silica reaction, efflorescence of calcium, lower soil/ water pH levels, etc. further exacerbate concrete degradation. The mechanical and chemical degradation of concrete catalyzes the corrosion of reinforcing bars upon internal exposure to waterborne chloride salts, or external exposure to airborne acidic gases after loss of concrete cover.

Reinforced concrete culverts are load-bearing drainage structures that must simultaneously ensure adequate hydraulic conveyance and maintain structural capacity under traffic loads. Their performance must therefore be evaluated in terms of both hydraulic adequacy and structural integrity. The objective of this research is to develop a dual risk assessment framework that independently quantifies two key serviceability risks: (1) hydraulic serviceability risk, influenced by mechanisms such as sedimentation, overtopping, and scouring; and (2) structural serviceability risk, driven by fatigue-induced cracking and chemical degradation. Both types of hazard will be modeled using network-level covariates to capture spatial and environmental variability. A rigorous comparison of six survival models will be performed using Akaike Information Criterion (AIC), log-likelihood values, and residual diagnostics, to identify the best-fitting model. Under the selected model, culvert-specific relative hazard estimates will be generated for both hydraulic and structural serviceability risks, supporting more targeted and effective infrastructure management decisions.

2. Methodology

Ordinarily, culverts are expected to serve at least for their design life if they deteriorate gradually. Therefore, their risk of failure can be assessed based on their deterioration speed (i.e., pace of aging) rather than simply their remaining useful life. The deterioration speed/ hazard rate measures the dynamic speed of failure at time t given that failure had not occurred by time t. In practical terms, it captures how quickly a culvert is aging or deteriorating at each moment, even if failure has not yet occurred.

If the consequences of serviceability failure are assumed to be similar across culverts, then relative risk comparisons can be made using hazard rates, which represent the instantaneous likelihood of failure at any given time. Hazard-based survival models, such as the Cox proportional hazards (PH) model, evaluate risk dynamically and conditionally over time without assuming a specific failure-time distribution. The Cox PH model estimates the influence of covariates on the hazard function while leaving the baseline hazard unspecified. This contrasts with life expectancy or probability-of-failure models, which typically rely on assumed failure-time distributions to estimate the average time to failure or cumulative risk. Such models produce scalar summaries (e.g., mean time to failure) and do not capture how failure risk evolves over time. As a result, they are less suitable for evaluating the time-varying nature of infrastructure deterioration.

Culverts serve two essential functions: supporting traffic loads without structural collapse and allowing sufficient water flow without over-topping the roadway. Accordingly, this study adopts a dual risk assessment framework to evaluate distinct functional risks that contribute to serviceability failure, namely structural weakness (e.g., material degradation, rebar corrosion) and hydraulic inadequacy (e.g., sedimentation, scouring, flooding).

2.1. Model Formulation

For a non-negative random variable T representing the time until failure, having a probability density function $f(t)$ and a cumulative distribution function $F(t)$, the probability that failure has occurred by duration t is defined as $F(t) = P\{T < t\}$. The probability of surviving beyond time t is denoted as the survival function Eq. (1 - 2). The survival function is the reverse cumulative distribution function of T. The distribution of T could also be equivalently characterized using the hazard function Eq. (3). The hazard function, or the rate of occurrence of failure at t, is defined as the conditional probability that failure occurs during $[t, t + \Delta t)$, given survival up to t, divided by the interval width, as expressed in Eq. (4). It could also be defined as the ratio of failure density to the survival probability, as derived in Eq. (5 - 8).

$$S(t) = P\{T \geq t\} = 1 - F(t) \tag{1}$$

$$S(t) = \int_t^{\infty} f(t)\Delta t \tag{2}$$

$$\lambda(t) = \lim_{\Delta t \to 0} \frac{P\{t \leq T < t + \Delta t \mid T \geq t\}}{\Delta t} \tag{3}$$

$$\lambda(t) = \lim_{\Delta t \to 0} \frac{P\{t \leq T < t + \Delta t\} \cap P\{T \geq t\}}{P\{T \geq t\} \ \cdot \Delta t} \qquad \text{(Conditional probability theorem)} \tag{4}$$

$$= \lim_{\Delta t \to 0} \frac{P\{t \leq T < t + \Delta t\}}{S(t) \ \cdot \Delta t} \tag{5}$$

$$= \lim_{\Delta t \to 0} \frac{F(t + \Delta t) - F(t)}{\Delta t} \cdot \frac{1}{S(t)} \tag{6}$$

$$= \frac{\partial F(t)}{\partial t} \cdot \frac{1}{S(t)} = \frac{\partial}{\partial t}\left((1 - S(t)) \cdot \frac{1}{S(t)}\right) \tag{7}$$

$$= \frac{f(t)}{S(t)} = -\frac{\partial}{\partial t} \ln S(t) \qquad \text{(Chain rule of differentiation)} \tag{8}$$

To assess the effect of covariates on culvert failure risk, the Cox PH model with Γ-distributed frailty was employed. Unlike fully parametric models, the Cox model does not require specification of a baseline hazard function, making it a semi-parametric model ideal for censored and time-to-event data, as commonly found in infrastructure asset management.

The hazard function represents the instantaneous risk of failure at time t, given survival up to that time. In a set of culverts indexed by $i; i \in \mathbb{Z}_+$, and exposed to r number of covariates, the Cox PH hazard function of culvert i with covariate vector $x_{(i,r)}$ is defined as $\lambda_i(t) = \lambda_o(t)\ exp\left(\beta^{\mathbf{T}} x_{(i,r)}\right)$, where $\lambda_o(t)$ is the baseline hazard and $\beta^{\mathbf{T}} x_{(i,r)}$ is the linear combination of covariates and their coefficients (i.e., $\beta_1 x_{(i,1)} + \beta_2 x_{(i,2)} + \cdots + \beta_r x_{(i,r)}$). The cumulative hazard function, $\Lambda(t)$, integrates the hazard over time Eq. (9), and the survival function, $S(t)$, gives the probability of surviving beyond time t Eq. (10). This shows that survival probability declines exponentially with cumulative hazard.

$$\Lambda(t \mid \mathbf{x}) = \int_0^t \lambda(u \mid \mathbf{x})\, \mathrm{d}u = \Lambda_0(t)\ \exp\left(\boldsymbol{\beta}^T \mathbf{x}\right) \tag{9}$$

$$S(t \mid \mathbf{x}) = \exp\left(-\Lambda(t \mid \mathbf{x})\right) = \exp\left(-\Lambda_0(t)\ \exp(\boldsymbol{\beta}^T \mathbf{x})\right) \tag{10}$$

Although the Cox PH model estimates the survival probability $S(t|x)$, it does not provide a closed-form expression for the expected survival time, or mean time to failure. The mean time to failure is defined as the integral of the survival function over time, $E[T|x] = \int_0^\infty S(t|x)\ dt$. However, since the Cox model does not specify the baseline survival function $S_o(t)$ parametrically, the integral cannot be evaluated analytically. In practice, the mean time to failure may be approximated numerically using the estimated survival curve, though for more direct interpretation of expected lifetimes, fully parametric models are preferred.

The hazard ratio (HR) compares the relative hazard between two culverts with covariate vectors differing by one unit in a specific covariate x_r. It is calculated as the ratio of their hazards Eq. (11). A hazard ratio greater than 1 indicates an increased risk of failure, while a value less than 1 indicates a protective effect of the covariate.

$$HR = \frac{\lambda(t|x+1)}{\lambda(t|x)} = exp\,(\beta_r) \tag{11}$$

The Cox model assumes that hazard ratios between individuals are constant over time. This PH assumption is fundamental to the model and implies that non-intersecting survival curves for different covariate profiles. Violations are tested with Schoenfeld residuals or time interaction terms. When the PH assumption is not satisfied for a specific categorical covariate, x_k, stratification allows the model to assign different baseline hazards to each category without estimating a coefficient for the stratified variable, while coefficients of other covariates are shared across all strata (i.e., effects of all other covariates remain the same). The stratified Cox model takes the form $\lambda_i(t|stratum\ x_k) = \lambda_{o,k}(t)\ exp(\beta^{\mathbf{T}} x_i)$, where the stratum-specific baseline hazard function $\lambda_{o,k}(t)$ varies across strata. This implementation improves robustness when key assumptions are violated.

Unobserved heterogeneity among culverts was modeled using a frailty term, ε_i. This random effect scales the individual hazard multiplicatively as $\lambda_i(t) = \varepsilon_i \cdot \lambda_o(t)\ exp\left(\beta^{\mathbf{T}} x_{(i,r)}\right)$. When $\varepsilon_i > 1$, the culvert is considered frail (more failure-prone), and when $\varepsilon_i < 1$, it is more robust. The frailty term is commonly assumed to follow a gamma distribution with mean 1 and variance θ. The gamma distribution is defined by the probability density function shown in Eq. (12). The individual survival function under frailty is $S(t \mid \varepsilon_i) = [S(t)]^{\varepsilon_i} = \exp(-\varepsilon_i \Lambda(t))$, which incorporates the effect of latent variable ε_i on survival. To obtain the marginal survival function for the population, ε_i is integrated out and expressed using cumulative hazard, yielding Eq. (13) and (14) respectively. These formulations allowed the Cox model to capture heterogeneity in risk across culverts due to unobserved or latent effects.

$$G(\varepsilon) = \frac{\varepsilon^{\left(\frac{1}{\theta}\right)-1}\, e^{-\frac{\varepsilon}{\theta}}}{\Gamma\left(\frac{1}{\theta}\right)\, \theta^{\frac{1}{\theta}}} \tag{12}$$

$$S(t \mid x) = \int_0^\infty [S(t)]^{\varepsilon_i}\, G(\varepsilon_i)\, d\varepsilon_i = [1 - \theta \ln S(t)]^{-\frac{1}{\theta}} \tag{13}$$

$$= \left[1 + \theta \Lambda_0(t) \exp(\beta^T x)\right]^{-\frac{1}{\theta}} \tag{14}$$

Estimation of model parameters was performed via maximum partial likelihood estimation, rather than full likelihood, because the baseline hazard $\lambda_o(t)$ remains unspecified in the Cox model. Unlike full likelihood estimation, partial likelihood focuses only on the relative ordering of failure times, which makes it robust under right-censoring. Let index j refer to the order of failure times and let the individual who fails at the observed failure time t_j be denoted by i_j. At each observed failure time t_j, the risk set $R(t_j)$ includes all individuals ℓ who are still at risk (i.e., have not yet failed or been censored) just prior to t_j. The conditional probability that culvert i_j fails at time t_j, given that one failure occurs at that time and conditioned on the risk set is shown in Eq. (15). The full partial likelihood over all D distinct observed failure times is given in Eq. (16). Taking the natural logarithm yields the log-partial likelihood Eq. (17), which is numerically maximized to estimate the regression coefficients β.

$$P(i \text{ fails at } t_j \mid \text{failure at } t_j) = \frac{\exp(\beta^{\mathbf{T}} x_{i_j})}{\sum_{\ell \in R(t_j)} \exp(\beta^T x_\ell)} \tag{15}$$

$$\mathcal{L}(\beta) = \prod_{j=1}^{D} \frac{\exp(\beta^{\mathbf{T}} x_{i_j})}{\sum_{\ell \in R(t_j)} \exp(\beta^{\mathbf{T}} x_\ell)} \tag{16}$$

$$l(\beta) = \sum_{j=1}^{D} \left[\beta^{\mathbf{T}} x_{i_j} - \log \left(\sum_{\ell \in R(t_j)} \exp(\beta^{\mathbf{T}} x_\ell) \right) \right] \tag{17}$$

This function was then numerically maximized, typically using the Newton-Raphson method, to obtain estimates for β. The Newton-Raphson method is a second-order iterative optimization procedure that uses both the gradient and the Hessian (second derivative) of the log-partial likelihood. At each iteration, the update rule is $\beta_{new} = \beta_{old} - \mathbb{H}^{-1}\mathscr{g}$ where $\mathscr{g}$ is the gradient and $\mathbb{H}$ is the Hessian evaluated at the current estimate. This method converges rapidly and is commonly used for estimating Cox model parameters. To handle ties, instances where multiple failures occur at the same time, the Breslow estimator was employed for estimating the partial likelihood. The Breslow approximation modified the denominator of the partial likelihood by treating tied failures as if they occurred sequentially but sharing the same risk set Eq. (18). This method aggregates the observed failures over time while adjusting for the risk set at each failure time using the estimated covariate effects. While this is an approximation, it is widely used due to its computational efficiency. The cumulative baseline hazard function $\hat{\Lambda}_o(t)$ was estimated for D_j set of individuals who failed at time t_j, and $d_j = |D_j|$ as presented in Eq. (19).

$$L_{\text{Breslow}}(\beta) = \prod_{j=1}^{D} \frac{\exp\left(\sum_{i \in D_j} \beta^{\mathbf{T}} x_i\right)}{\left(\sum_{\ell \in R(t_j)} \exp(\beta^{\mathbf{T}} x_\ell)\right)^{d_j}} \tag{18}$$

$$\hat{\Lambda}_o(t) = \sum_{t_j \le t} \frac{d_j}{\sum_{i \in R(t_j)} \exp(\beta^{\mathbf{T}} x_i)} \tag{19}$$

2.2. Independent Variables

The selection of independent variables was guided by identifying operating conditions that significantly affect the serviceability and performance of culverts, taking into account limitations in available network-level data. These variables were specifically chosen to evaluate two primary categories of serviceability risk: hydraulic inadequacy and structural weakness. Hydraulic inadequacy refers to the culvert's failure to convey water safely and efficiently under design or service conditions, which may result in localized flooding, sediment accumulation, upstream overtopping,

or channel erosion. Structural weakness, on the other hand, pertains to the deterioration or loss of mechanical integrity in the culvert structure, potentially compromising its ability to carry traffic loads and resist environmental degradation, even in the absence of outright structural failure.

The key factors affecting culvert hydraulics include: (a) head water and tail water depth; (b) cross-sectional shape and area of the culvert barrel; (c) inlet configuration; (d) barrel roughness; (e) barrel length; and (f) barrel slope. Among these, sedimentation, erosion, and flooding are closely associated with drainage-related variables such as peak flood discharge (Q), culvert slope (S), and barrel length (L). Peak flood discharge governs the hydraulic capacity requirements of a culvert (i.e., cross-sectional area and shape of the culvert barrel to convey stormwater safely). Slope influences velocity, affecting both sediment transport and erosion potential. Barrel length contributes to hydraulic head losses due to internal friction, especially in outlet-controlled culverts. Due to limited data on internal conditions (e.g., invert abrasion or sediment accumulation), the barrel roughness was not incorporated in the analysis.

The potential for structural weakness was assessed by examining factors that contribute to mechanical and chemical degradation of reinforced concrete culverts which are: traffic loading ($ADTT$), soil salinity (EC), and soil acidity (pH). Traffic loading induces fatigue stresses that can initiate cracking in the culvert structure, while saline or acidic soil/ water conditions can exacerbate chemical deterioration of concrete. In this framework, the variables Q, S, and L were used to assess the risk of hydraulic inadequacy (Scenario 1), whereas $ADTT$, EC, and pH were employed to evaluate the potential for structural weakening (Scenario 2). During the analysis, it was assumed that culvert fill cavitation and differential settlement were negligible for all culverts. It was also assumed that annual fluctuations in peak discharge were minimal, and that the natural alignment of the drainage channel remained unaltered during culvert construction.

The design peak discharge represents the maximum flow rate corresponding to a defined probability or return period, as specified for drainage infrastructure by the Ethiopian Roads Authority (ERA) [1]. Direct runoff represents the portion of precipitation that reaches stream channels shortly after a storm, following initial losses due to interception, infiltration, evaporation, and surface storage. To estimate this runoff for ungauged basins, ERA adopts the Soil Conservation Service (SCS) Curve Number (CN) method. This empirical method estimates runoff volume based on precipitation, land use, soil type, and Antecedent Moisture Condition (AMC) [3]. Accordingly, runoff depth Q was computed as a function of average daily precipitation P and CN value associated with the hydrologic soil group and land use at each site, as shown in Eq. (20).

$$Q = \frac{\left(P - 0.2\left(\frac{254000}{CN} - 254\right)\right)^2}{P + 0.8\left(\frac{254000}{CN} - 254\right)} \tag{20}$$

The fatigue loading variable was based on a standard axle configuration defined in the ERA bridge design specification [4], where loading frequency is represented by the single-lane average daily truck traffic $ADTT_{SL}$ Eq. (21).

$$ADTT_{SL} = \rho \cdot ADTT \tag{21}$$

Where:

- $ADTT$: The number of trucks per day in one direction.
- ρ: Fraction of traffic in a single lane, specified as 1.00, 0.85, and 0.80 for culverts with 1, 2, and more than 3 lanes, respectively.

The culvert slope was derived from Digital Elevation Model (DEM), as it generally aligns with the natural gradient of the stream channel unless the culvert inlet is raised or lowered due to clearance conflicts, which is atypical of cross-regional trunk roads. Similarly, barrel length was also taken as-is from available records. Soil pH, measured at a depth 1 meter, was used to represent the acidity or alkalinity of the surrounding environment. Electrical Conductivity (EC), expressed in deci Siemens per meter (dS/m) from a 1:x soil-to-water solution, quantified the concentration of dissolved salt ions in soil moisture and served as a standard indicator of soil salinity.

3. Data Preparation

This study analyzed a total of 2,190 cast-in-situ reinforced concrete slab and box culverts located across Ethiopia. The dataset, sourced from ERA, details the type, location, geometric feature, age, and traffic count of the culverts. Failure events, treated as non-censored observations, were identified from ERA's records of culvert replacements attributed to failure.

Geospatial inputs for runoff depth estimation comprised the ASTER GDEM V3 30m resolution digital elevation model [5], the FAO Digital soil map [6], wet-season precipitation from the IWMI [7], and the MODIS MCD12Q1 V6.1 land-use/land-cover dataset [8] (Fig. 2A–D). Curve numbers were assigned according to the TR-55 standard tables for various land use and hydrologic soil group combinations, as specified in Chapter 2, Tables 2-2a through 2-2d of the USDA Technical Release 55 manual [3]. These empirically derived values reflect runoff potential based on land cover characteristics and soil infiltration capacity. A spatially distributed CN grid was generated by integrating land cover (i.e., classified into 17 International Geosphere-Biosphere Programme (IGBP) categories [9]) with hydrologic soil group data under average moisture conditions (AMC II) (Fig. 3). A weighted CN value was calculated for each culvert's delineated catchment. The four hydrologic soil groups in the CN method are A, B, C, and D, each categorized by infiltration rate and runoff potential. Group A includes gravelly or sandy soils with high infiltration rates and minimal runoff (typically AMC I). Group B comprises coarse to fine silt loam soils with moderate infiltration rates (AMC II). Group C consists of fine-textured soils such as sandy clay loam with slow infiltration under saturated conditions (AMC III). Group D includes soils with very low infiltration, high runoff potential, and often features such as high-water tables, claypans, saline crusts, or even water bodies.

Ethiopia's wet season, spanning mid-June to mid-September (approximately 90 days), accounts for 50–80% of annual rainfall. Daily precipitation (P) was calculated by averaging total wet season rainfall over the 90-day period. Runoff depth (Q) was then estimated using the SCS runoff equation (20). DEM data were utilized to delineate catchment boundaries. However, further hydrologic computations, such as runoff volume estimation or unit hydrograph development, were not pursued due to the lack of stream gauge measurements and the absence of channel geometry data (e.g., wetted perimeter) required for flow velocity estimation. Methods such as the Kirpich formula were deemed incompatible with the assumptions underlying the SCS method.

The fatigue load variable was derived from average daily truck traffic counts, with the single-lane truck frequency computed as per the ERA bridge design specification [4]. Culvert barrel

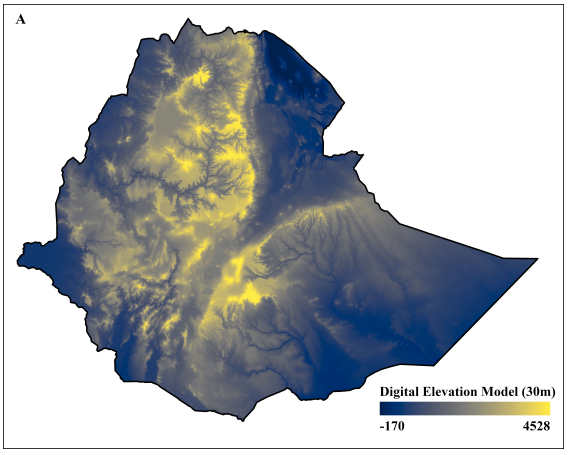

A. ASTER V3 30 m Digital Elevation Model

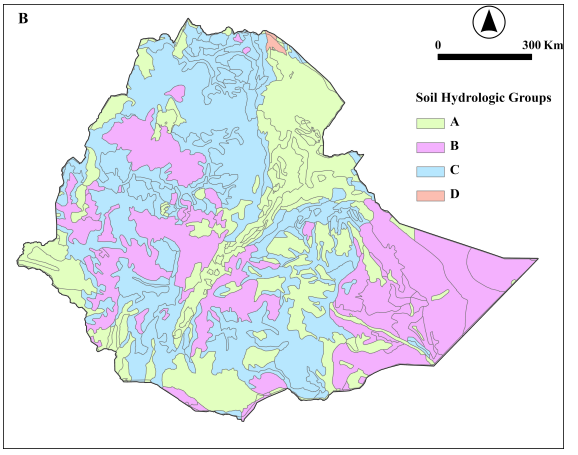

B. Soil Hydrologic Group Classification

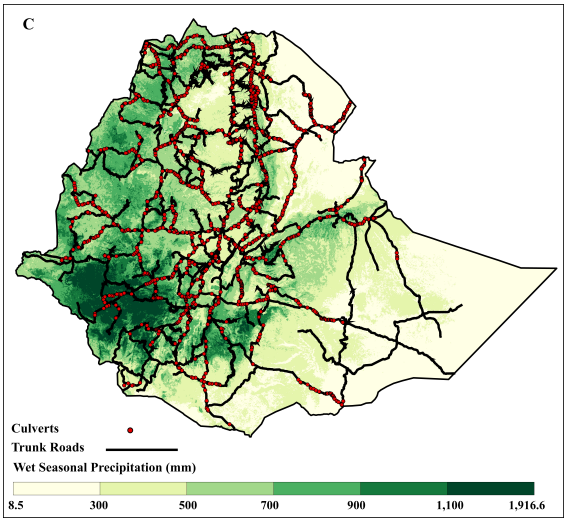

C. Wet Season Precipitation

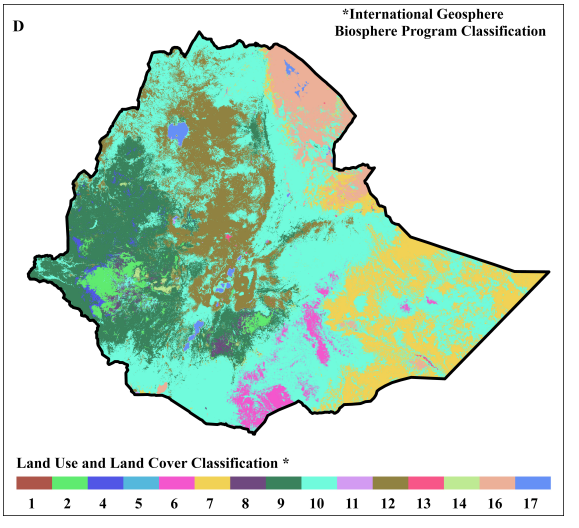

D. MCD12Q1 V6.1 Land Use Classification

Figure 2: Inputs for peak seasonal flood depth estimation

lengths ranged from 4 to 320 meters. Culvert slopes (%) were extracted from the DEM, under the assumption that natural channel profiles remained undisturbed by construction. According to the ERA's geometric design manual terrain classification [10], the culverts are situated in flat (78.50%), rolling (16.49%), mountainous (4.26%), and escarpment (0.75%) terrain classes (Fig. 4).

Subsurface chemical exposure was assessed using two indicators: soil pH and electrical conductivity (EC). Soil pH at a depth of 1 meter [11] characterized the acidity or alkalinity of the surrounding soil, which affects concrete degradation (Fig. 5). EC values, expressed in dS/m from a 1:x soil-to-water solution and sourced from [11], indicated salinity levels (Fig. 6). The EC data were interpreted using salinity index classifications from the USDA Soil Survey Manual [12].

Prior to analysis, a series of data cleaning and preprocessing steps were applied to improve data quality and ensure interpretability. Outliers were removed from all covariates using the Interquartile Range (IQR) method. This helped mitigate the influence of extreme values that could bias results

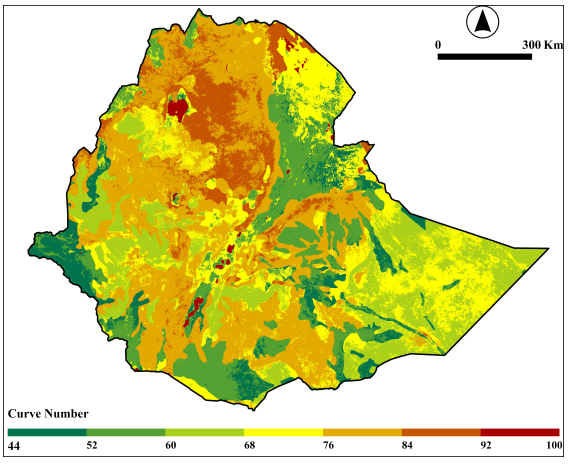

Figure 3: Curve number classification

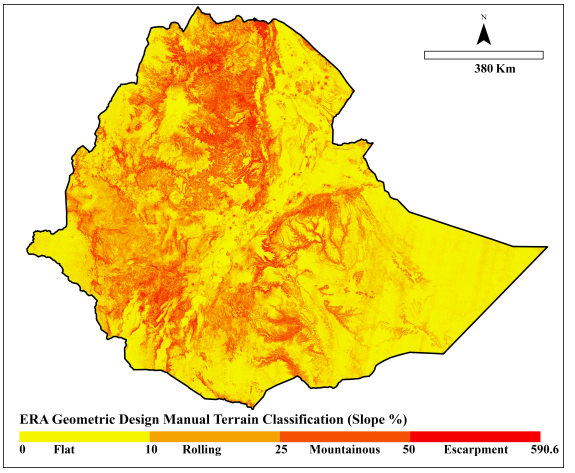

Figure 4: Slope (%)

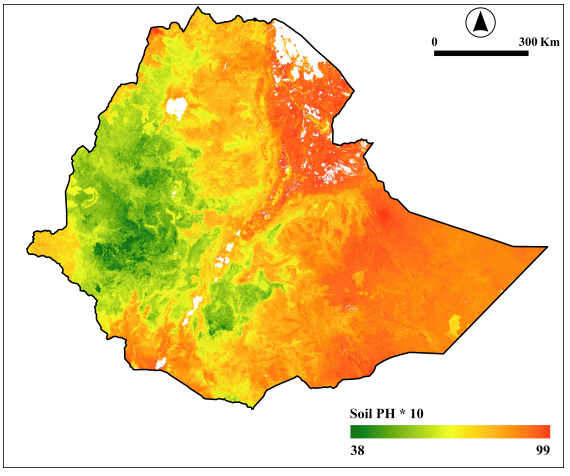

Figure 5: Soil pH

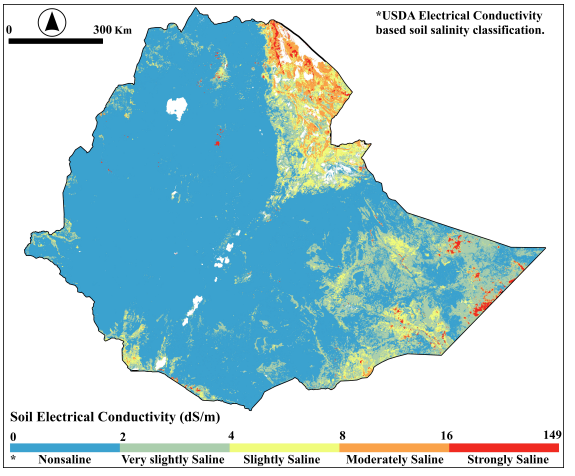

Figure 6: Soil Salinity

or reduce statistical reliability. After outlier removal, all covariates were standardized using z-score normalization, setting the mean to zero and standard deviation to one, which improved numerical consistency and facilitated comparison across variables. Multicollinearity was assessed using the Variance Inflation Factor (VIF), and all predictors showed VIF values below 1.2, confirming that no significant collinearity existed. Although EC and pH exhibited a statistically significant moderate correlation ($r = 0.34, p < 0.0001$) (Fig. 7), this relationship did not pose a multicollinearity concern given their low VIF values, which were 1.13 for EC and 1.16 for pH.

4. Results

Two parallel failure scenarios were defined for the analysis. Scenario 1 (hydraulic inadequacy hazard) models the time to first hydraulically driven serviceability loss, such as overtopping, sediment blockage, or scour, using discharge depth (Q), culvert slope (S), and barrel length (L). Scenario 2 (structural weakness hazard) models the time to first structurally driven serviceability

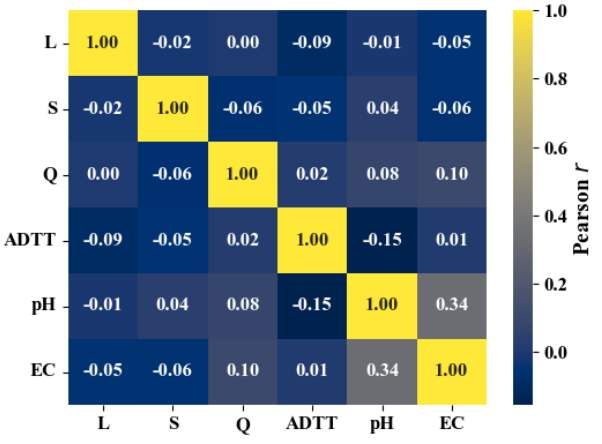

Figure 7: Covariate correlation matrix

loss, such as fatigue cracking or delamination, using average daily truck traffic ($ADTT$), soil pH, and soil salinity (EC).

Six survival models were evaluated under varying distributional assumptions: Γ-frailty Cox PH, Weibull, Log-Normal, Log-Logistic, Aalen's additive, and piecewise exponential as shown in Appendix A. The Cox PH model emerged as the most appropriate model for both scenarios, achieving the lowest Akaike Information Criterion (AIC) and highest log-likelihood, indicating superior statistical fit. While Aalen's additive model could not be compared via likelihood-based metrics, martingale residual diagnostics showed systematic underestimation of hazard, especially at later times, indicating its additive hazard form could not scale with aging infrastructure. In contrast, martingale residuals for the Cox model were well-centered, supporting its adequacy. These findings justified the selection of Γ-frailty Cox model as the best fit for the studied culvert dataset.

Further diagnostics using Schoenfeld residuals confirmed the Cox model's adequacy for most covariates. However, EC violated the PH assumption, prompting stratification by EC groups. While this partially improved curve behavior, log–log survival plots still showed non-parallelism and crossing, indicating that stratification alone was insufficient. Kaplan–Meier curves paradoxically showed longer survival for culverts in high EC zones; contradicting expectations based on salinity-driven degradation. This counterintuitive finding was attributed to multiple confounders: a moderate correlation between EC and pH, sampling bias due to limited high-EC representation, right-censoring of younger culverts in saline areas, and possibly better construction or maintenance in these zones. As these issues undermined EC's causal interpretation and violated model assumptions, EC was excluded from the final Cox model to enhance validity and robustness of the hazard estimates.

In the final Γ-frailty Cox PH model estimate Table 1, slope (S) retained a statistically significant negative association with hydraulic-inadequacy hazard. This indicates that steeper culverts are $\approx 15\%$ less likely to experience hydraulic malfunction, plausibly because higher gradients enhance self-cleaning and reduce sediment build-up. Conversely, gentler slopes may promote sediment deposition, which can obstruct flow and increase mechanical stress on the structure. Culvert length (L) showed a modest, non-significant protective effect, while discharge depth (Q) had no discernible effect. All hydraulic hazard ratios fall below 1, reinforcing the interpretation that higher

Table 1: Γ-frailty Cox PH Estimates: Hydraulic inadequacy vs. Structural weakness scenarios

Scenario 1					**Scenario 2**				
Covariate	β	HR	95% CI	p-value	Covariate	β	HR	95% CI	p-value
L	−0.120	0.887	0.755–1.040	0.140	$ADTT$	+0.237	1.267	1.100–1.460	0.001
S	−0.163	0.849	0.722–0.999	0.049	pH	−0.146	0.864	0.761–0.982	0.025
Q	−0.044	0.957	0.818–1.119	0.583					

EC was excluded from the Cox model due to its constant violation of the PH assumption.
β values are log-hazard coefficients; $HR = e^{\beta}$. Confidence bounds are $\beta \pm 1.96\,SE$, with SE as the standard error.

design-parameter values tend to suppress failure risk and suggesting hydraulic inadequacy is not the predominant cause of failure within the studied culvert population. These findings may reflect the adequacy of current hydraulic design standards in mitigating flow-related risks under the conditions observed in this dataset.

For the structural-weakness hazard, average daily truck traffic ($ADTT$) emerged as a strong risk amplifier. A one-standard-deviation increase in truck frequency elevated the instantaneous structural-failure hazard by approximately 27%, aligning with expectations of cumulative fatigue damage. Conversely, soil pH exerted a statistically significant protective effect. A one-standard-deviation rise in pH, indicating a shift toward a more alkaline environment, reduced the instantaneous structural-failure hazard by roughly 14%. This finding suggests that more alkaline soils mitigate hazard rates, likely due to lower corrosion activity and slower material degradation under less acidic conditions. Collectively, these results confirm that structural vulnerability is primarily governed by the combined influence of loading intensity and environmental exposure, underscoring the importance of accounting for both traffic-induced stresses and corrosive environments in culvert maintenance and management strategies.

Figure 8 supports and expands on the model findings. Both serviceability hazards accumulate slowly until around 60-70 years, then jump more sharply thereafter. Scenario 1 shows a slightly earlier and steeper rise in hazard accumulation, beginning around 40 years, and climbing rapidly between 70-90 years. It eventually plateaus near a cumulative hazard of 0.42 by 100 years. In contrast, Scenario 2 closely tracks Scenario 1 until about 70 years but then increases more gradually, leveling off around 0.40. Throughout, the hydraulic inadequacy hazard lies slightly above the structural weakness hazard, indicating that, on average, hydraulic inadequacy driven failures tend to emerge earlier in the lifecycle, necessitating earlier inspection and maintenance. Conversely, the slower cumulative hazard accumulation in Scenario 2 aligns with gradual structural degradation, where damage accrues over prolonged exposure to load and environmental stressors, which may justify slightly longer intervals before intensive inspection for structurally induced risk.

The stratified Kaplan–Meier survival curves (Fig. 8) confirm that hydraulic and structural covariates drive culvert survival in intuitive ways: in Scenario 1, flatter and longer culverts ("Low S" and "High L") see more rapid declines in survival, reflecting increased risk of sediment blockage, overtopping, and head-loss, while higher discharge capacity provides only marginal protection. In Scenario 2, culverts experiencing heavier daily truck traffic and more acidic soils ("High $ADTT$" and "Low pH") lose survival probability markedly faster, consistent with

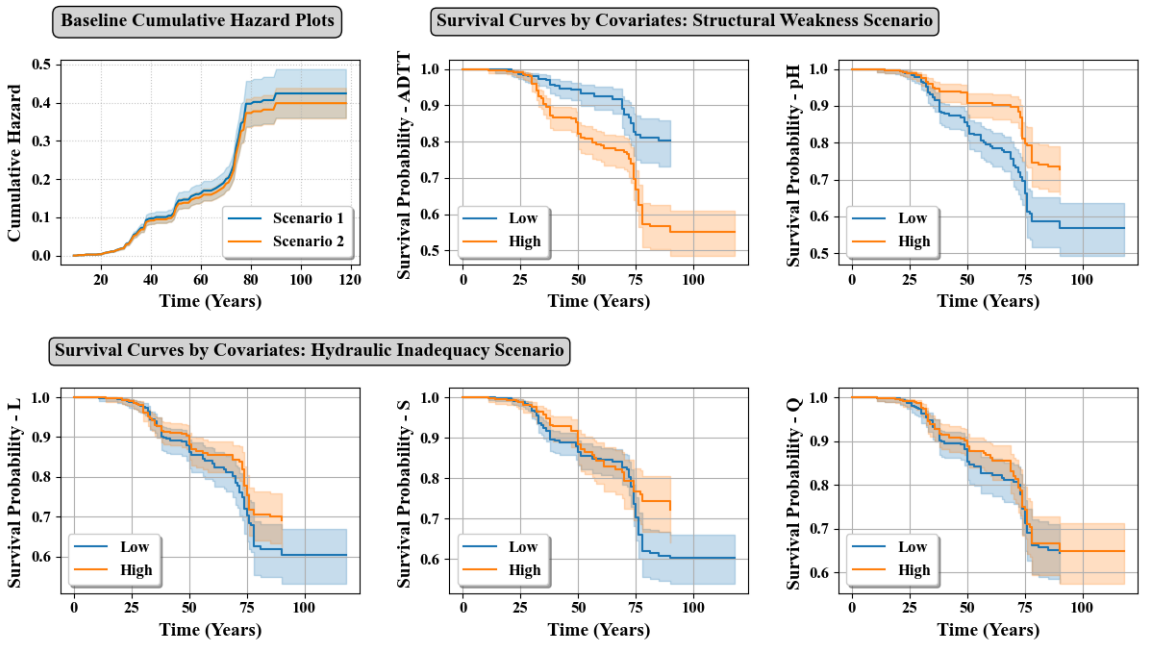

Figure 8: Baseline cumulative hazard and covariate-stratified survival curves with 95% CI

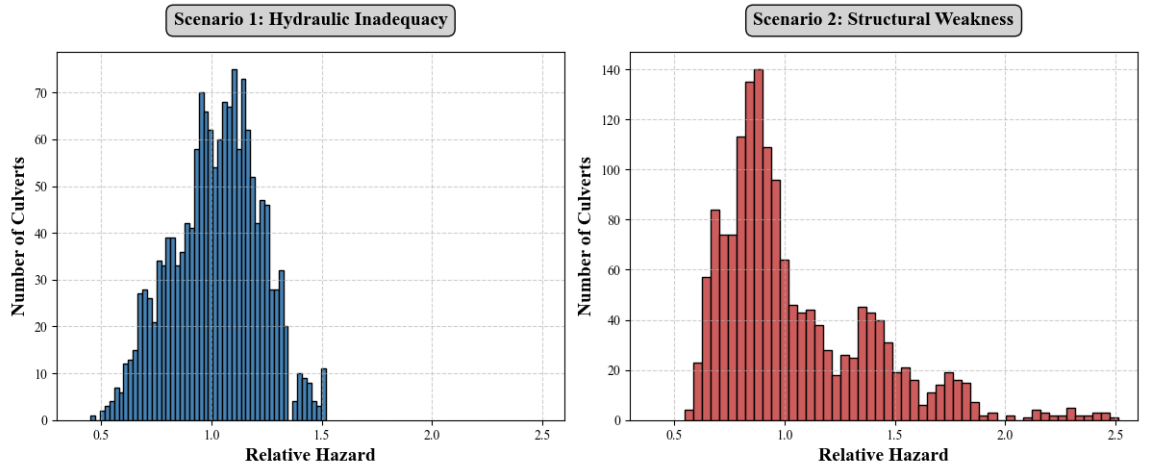

Figure 9: Histograms of relative hazard estimates for individual culverts

cumulative fatigue damage and accelerated chemical degradation. These patterns mirror the frailty-Cox estimates (e.g., $HR = 0.85$ for slope, $HR = 1.27$ for $ADTT$, $HR = 0.86$ for pH) and suggest that inspection resources should be prioritized toward flat, long culverts for hydraulic checks and high-traffic, low-pH sites for structural assessments.

The histograms of individual hazard rates (Fig. 9), derived from the Γ-frailty models, reveal the distribution of relative risk across culverts for both scenarios. In Scenario 1, relative hazards span roughly 0.7–1.3, peaking near 0.95 with a mild right-hand skew, indicating that while most culverts experience moderate hydraulic vulnerability, a few sites are considerably more susceptible.

In contrast, Scenario 2 exhibits a tighter cluster of hazard rates, with a primary mode around 0.9–1.0 and smaller secondary peaks at 1.4–1.6. This tighter clustering reflects the broadly uniform structural risk across the network, with culverts along similar routes sharing comparable truck-loading and material properties. A subset of culverts (those under very heavy daily traffic or in more acidic soils) face substantially higher failure hazards. Overall, hydraulic risk appears more dispersed across the network, whereas structural risk is relatively homogeneous yet laced with pronounced extremes.

5. Conclusions

This study has developed and validated a data-driven, dual-hazard framework for estimating serviceability risks in reinforced concrete culvert networks, treating hydraulic inadequacy and structural weakness as distinct yet interrelated failure modes. By modeling these risks separately, the framework offers a more granular understanding of failure mechanisms, enabling targeted inspection strategies aligned with the unique temporal and physical characteristics of each hazard.

A rigorous comparison of six survival models using Akaike Information Criterion, log-likelihood, and residual diagnostics identified the Γ-frailty Cox PH model as the best-fitting approach for both hazard scenarios. This semi-parametric, frailty-adjusted formulation proved well-suited to censored, heterogeneous culvert datasets, effectively accounting for unobserved heterogeneity across the network.

In the hydraulic hazard model, barrel slope emerged as the only covariate with a statistically significant protective effect, with all hydraulic hazard ratios falling below one, indicating that steeper gradients suppress failure risk. Discharge depth and barrel length did not exhibit discernible effects. These results suggest that current hydraulic design standards are generally effective under observed conditions; however, flatter, longer culverts remain susceptible to sedimentation and overtopping and therefore warrant earlier and more frequent inspection.

In contrast, the structural hazard analysis identified average daily truck traffic as a strong risk amplifier, while higher soil pH was associated with reduced risk, emphasizing the combined role of loading intensity and environmental corrosivity in degrading structural integrity. Soil electrical conductivity was excluded from the final model due to persistent violations of the PH assumption, underscoring the importance of rigorous diagnostic validation in survival model development.

Cumulative hazard plots revealed only modest temporal differences between the two hazard types. Failures due to hydraulic inadequacy tended to emerge slightly earlier in the service lifecycle, while structural deterioration accumulated more gradually, though at a comparable overall rate. This modest but meaningful temporal divergence between hazard types, where hydraulic inadequacy tends to manifest slightly earlier and structural deterioration accumulates more gradually, supports differentiated inspection strategies.

Distributions of individual hazard rates revealed greater variability in hydraulic risk, which was more spatially dispersed across the network. Structural risk, by contrast, exhibited relative uniformity, reflecting similar traffic loading patterns among culverts along shared routes, but was punctuated by localized extremes where high truck volumes and acidic soils converge. This clustering underscores the importance of spatially targeting structural assessments to these high-risk subpopulations.

These insights carry direct implications for inspection planning and maintenance optimization. Resources should be directed toward hydraulic assessments of long, flat culverts where flow-related failures emerge earlier, while structural evaluations should focus on sites with heavy truck traffic and low soil pH. By aligning inspection targets and timing with the distinct progression patterns of hydraulic and structural hazards, infrastructure managers can improve preventive maintenance outcomes and allocate inspection resources more efficiently.

Beyond practical applications, this work affirms the methodological suitability of frailty-adjusted Cox PH models for infrastructure serviceability risk assessment using hazard-specific covariates. Future research should explore the incorporation of time-varying covariates, the application of this dual-hazard framework to other asset classes, and the integration of cost-effectiveness analyses to refine inspection intervals under budgetary constraints.

Acknowledgements

The authors thank Ethiopian Roads Authority for the reinforced concrete culvert dataset and appreciate the freely available public data sources that supported this research. Mearg N. Sahle, in particular, gratefully acknowledges Zachery Taylor Howell for providing essential computing resources and extends heartfelt gratitude to Kidus Michael for unwavering support and encouragement throughout this work.

Data Availability Statement

The environmental datasets used in this study are publicly accessible from their respective online repositories. The culvert dataset, containing information on type, location, geometry, age, traffic counts, and records of replacement due to failure, was obtained from the Ethiopian Roads Authority under official permission. Due to data use restrictions, this dataset is not publicly distributable. Researchers interested in accessing the culvert data for verification or further analysis may contact the Ethiopian Roads Authority directly, subject to their review and approval.

Declaration of Competing Interest

The authors declare that they have no known competing financial interests or personal relationships that could have appeared to influence the work reported in this paper.

Funding Sources

This research was supported in part by the Ministry of Education, Culture, Sports, Science and Technology (MEXT) of Japan through the Japanese Government (MEXT) Scholarship Program, awarded to Mearg Ngusse Sahle. The authors also acknowledge institutional support provided by Osaka University. The funding source had no involvement in the study design, data collection, analysis, interpretation of data, writing of the manuscript, or the decision to submit the article for publication.

A. Survival Diagnostics and Model Fit Assessment

In survival analysis, assuming a specific distribution for survival times requires careful consideration to avoid misleading inferences. Therefore, various distributional assumptions were

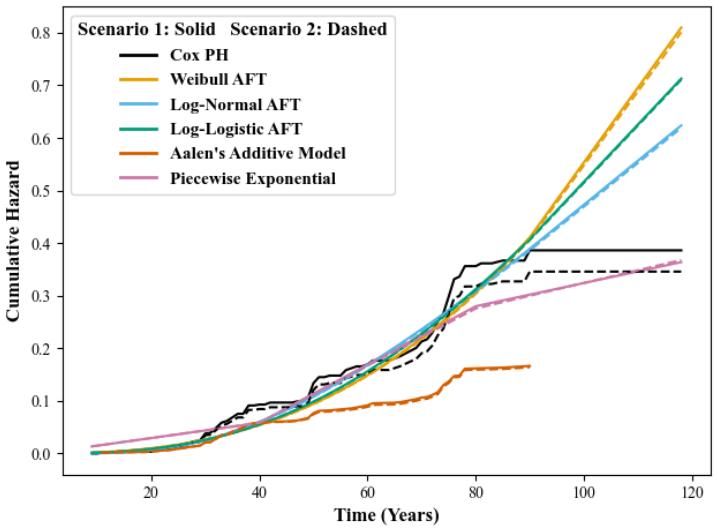

Figure 10: Cumulative hazard plots

evaluated to identify the most appropriate culvert-survival model. Table 2 summarizes each specification and its associated survival time equation.

Table 2: Distributional assumptions of candidate survival models

Model	**Functional form**	**Survival function** $S(t)$	**Hazard function** $h(t)$
Weibull AFT	(λ, γ)	$\exp\left[-(\lambda t)^{\gamma}\right]$	$\lambda^{\gamma}\,\gamma\,t^{\gamma-1}$
Log-Normal AFT	(μ, σ)	$1-\Phi\left(\frac{\ln t-\mu}{\sigma}\right)$	$\frac{\phi\left(\frac{\ln t-\mu}{\sigma}\right)}{\sigma\,t\,[1-\Phi(\cdot)]}$
Log-Logistic AFT	(α, γ)	$\frac{1}{1+(t/\alpha)^{\gamma}}$	$\frac{\gamma\,(t/\alpha)^{\gamma-1}}{\alpha\,[1+(t/\alpha)^{\gamma}]}$
Aalen additive	$h(t \mid X)=\alpha_0(t)+\beta^T(t)X$	$\exp\left[-\int_0^t\{\alpha_0(s)+\beta^T(s)X\}\,ds\right]$	$\alpha_0(t)+\beta^T(t)X$
Cox PH (Γ-frailty)	$h(t \mid X)=\varepsilon\,h_0(t)\,e^{\beta^T X}$	$\left[1-\theta\ln S_0(t)\,e^{\beta^T X}\right]^{-1/\theta}$	$\varepsilon\,h_0(t)\,e^{\beta^T X}$
Piecewise exponential	$h(t)=\lambda_j$ on $[t_{j-1}, t_j)$	$\exp\left[-\sum_j \lambda_j\,\Delta t_j\right]$	λ_j (interval constant)

Fully parametric Accelerated-Failure-Time (AFT) forms (Weibull, Log-Normal, Log-Logistic), the piecewise-exponential model, the semi-parametric Cox Proportional-Hazards (PH) and Aalen's additive models were all fitted for both scenarios, and their baseline cumulative-hazard curves compared (Fig. 10). For the piecewise exponential model, breakpoints were set at 40 and 60 years. Among the fitted models, the Cox model, with its baseline hazard estimated non-parametrically using Breslow's estimator, achieved the highest (least-negative) log-likelihood and the lowest Akaike Information Criterion (AIC) Table 3, whereas the additive model, lacking a likelihood, required purely graphical scrutiny. Although Aalen's additive model is valuable when proportionality is

violated or when absolute hazard increments are of particular interest, its coefficients are less intuitive, more sensitive to outliers, and unsupported by standard information criteria. Consequently, when the PH assumption is plausible, the Cox model remains the preferred framework.

Table 3: Model fit comparison

Rank	Model	Scenario 1		Scenario 2	
		AIC	Log-likelihood	AIC	Log-likelihood
1	Cox PH	1640.50	-817.25	1619.08	-806.54
2	Log-Normal AFT	2554.91	-1272.45	2556.54	-1273.27
3	Log-Logistic AFT	2565.07	-1277.53	2568.86	-1279.43
4	Weibull AFT	2569.78	-1279.89	2575.44	-1282.72
5	Piecewise Exponential	2715.12	-1345.56	2717.27	-1346.63
×	Aalen's additive	N/A	N/A	N/A	N/A

Goodness-of-fit was further examined with the martingale residuals, defined for each subject as $r_i = \delta_i - \widehat{H}_i(T_i)$, where δ_i is the event indicator and $\widehat{H}_i(T_i)$ is the model-predicted cumulative hazard at that subject's observed time T_i. For the Cox model (Fig. 11), event residuals clustered near zero and censored residuals were symmetrically centered below zero (i.e. balanced risk estimation), indicating that the fitted cumulative-hazard surface captures most of the observed risk (i.e., the model already attributes roughly half of the observed risk to the covariates). In contrast, the additive model left almost every event with $r_i \approx 1$ signaling systematic under-prediction (i.e., the model claims only $< 25\%$ of the hazard,the 75% remains unexplained) (Fig. 11). The systematic time trend in the Aalen's residuals is evidence that strictly additive hazard structure fails to scale with aging, Cox's multiplicative structure fares better. These graphical findings agree with the numerical criteria, confirming the superior fit of the Cox specification.

The martingale-residual plot for the Cox model is generally well-centered across most follow-up times, indicating good overall model fit. However, a fan-like divergence emerges near 80 years, suggesting that the model underestimates the cumulative hazard for a subset of long-surviving culverts. This pattern points to potential time-dependent covariate effects and possible violations of the PH assumption. To investigate the source of this misfit, scaled Schoenfeld residuals were computed for the covariates in the separate Cox specifications representing the hydraulic-risk and structural-risk scenarios.

Scaled Schoenfeld residual plots are commonly used to evaluate the PH assumption in Cox regression models by visually examining how residuals, representing the difference between observed and predicted event times, vary over time for each covariate. For a subject experiencing an event at time t_i, the scaled Schoenfeld residual for covariate r is computed as shown in Eq. (22, 23), where $\widehat{\sum}_{rr}$ is the r^{th} diagonal element of the estimated variance-covariance matrix of the fitted coefficient vector $\hat{\beta}$, and $\bar{x}_r(t_i)$ is the risk-set weighted average of the covariate at time t_i.

$$\omega_{i,r}^{\text{scaled}} = \widehat{\sum}_{rr} \left[x_{ir} - \bar{x}_r(t_i) \right] \tag{22}$$

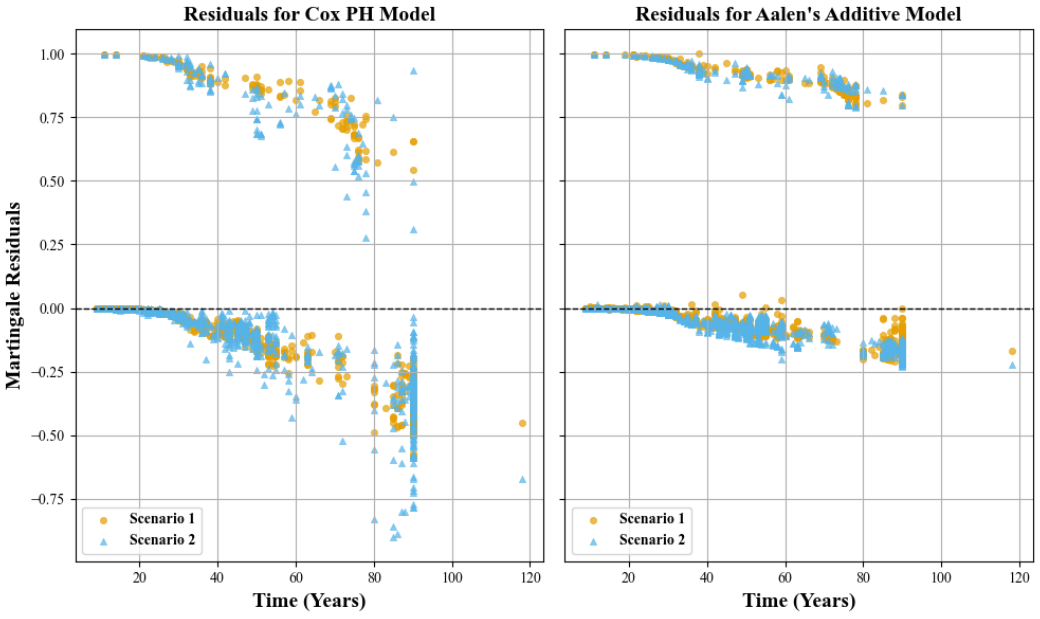

Figure 11: Martingale residuals – Cox PH and Aalen's Additive

$$\bar{x}_r(t_i) = \frac{\sum_{k\in\Omega(t_i)} x_{kr} \exp\left(\hat{\beta}^T X_k\right)}{\sum_{k\in\Omega(t_i)} \exp\left(\hat{\beta}^T X_k\right)} \tag{23}$$

Under the PH assumption, the scaled Schoenfeld residuals $\omega_{i,r}^{\text{scaled}}$ should exhibit no systematic trend with t_i. When plotted against event times, these residuals should appear randomly scattered around zero, without systematic trends, indicating that covariate effects are constant over time. Any clear temporal drift therefore reveals the covariate(s) whose effects change over time, explaining the late-time martingale spike, and indicating the need for stratification or explicit time-dependent interaction terms. In this study, the PH assumption was upheld for all covariates in Scenario 1 (L, S, Q) and for $ADTT$ and pH in Scenario 2, as supported by non-significant p-values ($p > 0.05$) and residual plots showing random scatter over time (Fig. 12). However, EC in Scenario 2 violated the PH assumption significantly ($\chi^2 = 1.55, p = 0.01$), with residual plots exhibiting a wider vertical spread and a potential increasing effect at later times. This means the hazard ratio for the covariate might change as time progress.

To address this violation, EC was treated as a stratification variable, allowing for distinct baseline hazards across EC strata without altering the coefficients of other covariates. The effectiveness of stratification was further examined through log-log survival plots($\log\left(-\log S(t)\right)$ vs. $\log t$), a diagnostic tool that visually assesses the PH assumption by examining whether survival functions across strata exhibit parallelism over time, as presented in (Fig. 13). When plotted for finely resolved individual levels, the survival curves appeared erratic and markedly non-parallel, confirming violations of the PH assumption, likely attributable to small sample sizes or sparse failure events within certain EC strata. While aggregating EC into Low, Medium, and High groups improved curve stability; the stratified log-log plots still exhibited evident non-parallelism and

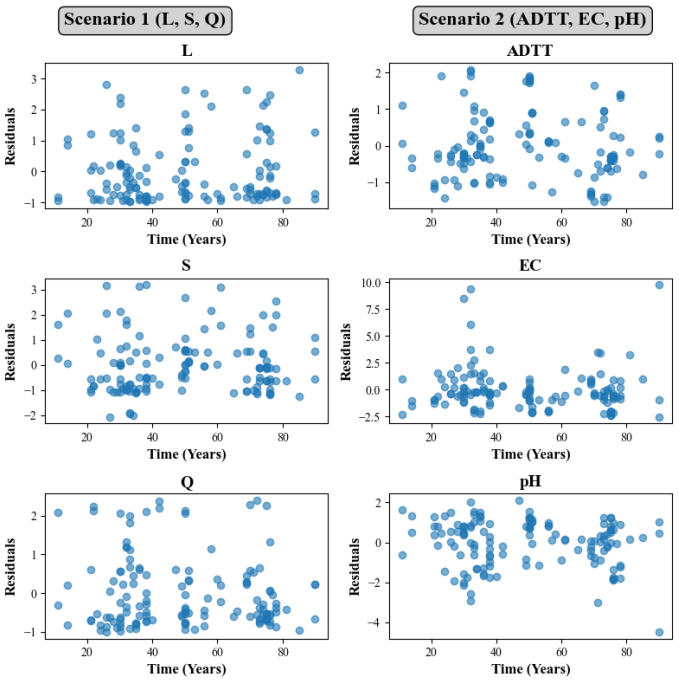

Figure 12: Cox model PH assumption test: Plots of Scaled Shoenfeld residuals

Table 4: Cox PH assumption test results for Scenario 1 and 2

Scenario 1: Hydraulic Failure Risk			**Scenario 2: Structural Failure Risk**		
Covariate	χ^2	P-value	Covariate	χ^2	P-value
L	0.69	0.41	$ADTT$	0.04	0.84
S	0.18	0.67	EC	1.55	0.01
Q	1.10	0.29	pH	2.29	0.13

curve crossings, most notably, early divergence in the Low EC group (i.e. culverts in low EC group start failing) and unstable spacing between Medium and High EC groups. These features suggested that the PH assumption remains violated even under coarser stratification.

Complementary evidence from Kaplan-Meier survival curves in (Fig. 14) also revealed a counterintuitive trend: higher EC levels, commonly associated with elevated soil salinity and expected to accelerate concrete degradation, were instead linked to longer culvert survival times. This paradox may be explained by several confounding influences: (a) a moderate yet statistically significant correlation between EC and pH ($r = 0.34, p < 0.0001$), which, despite low multicollinearity (VIFs of 1.13 and 1.16), suggests overlapping soil chemical characteristics; (b) sampling bias, as most culverts in the dataset are located in zones with salinity index values below 2, potentially limiting representation of more corrosive environments; (c) informative censoring due to culvert age, since structures in high EC zones tend to be relatively new and have not yet experienced failure, resulting in an apparent protective effect that reflects insufficient

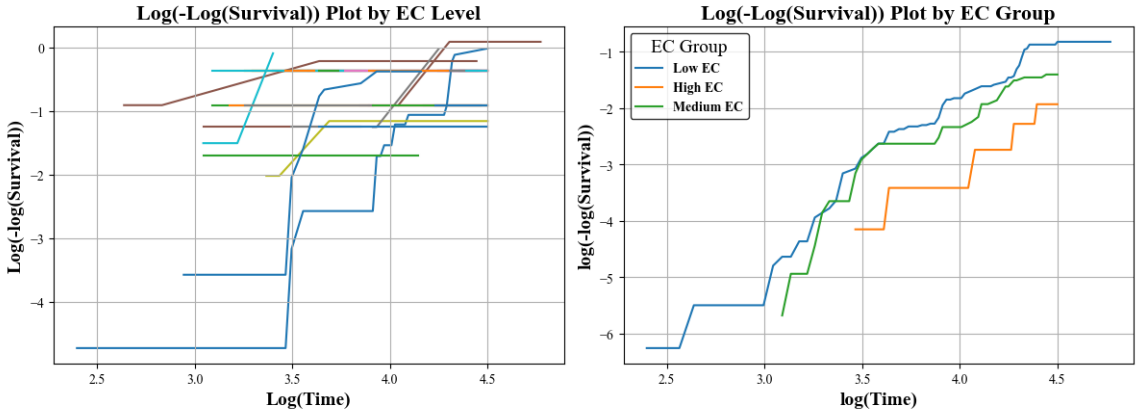

Figure 13: Log-Log Survival Curves for *EC* Levels: Comparison of Individual and Grouped Strata

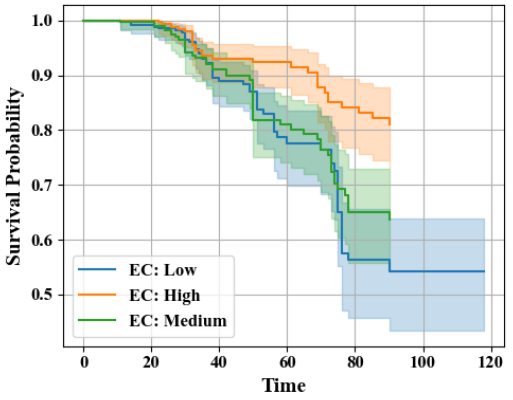

Figure 14: Survival Probability of Culverts by EC Tertiles: Kaplan-Meier Estimates

exposure time rather than true durability; and (d) the possibility that culverts in saline-prone areas benefit from superior construction practices or more frequent maintenance interventions. Taken together with persistent violations of the PH assumption observed in log–log survival plots, these inconsistencies undermine the causal interpretability of *EC* within the Cox model. Therefore, *EC* was excluded from the final model to improve statistical validity, parsimony, and adherence to model assumptions, ensuring more reliable estimation of hazard effects.

CRediT authorship contribution statement

Mearg Ngusse SAHLE: Conceptualization, Methodology, Software Development, Formal Analysis, Investigation, Validation, Visualization, Writing – Original Draft. **Zachery Taylor HOWELL:** Resources, Data Curation, Software Development.

References

[1] Ethiopian Roads Authority, Drainage Design Manual, 2013.
[2] American Association of State Highway and Transportation Officials, AASHTO LRFD Bridge Design Specifications, 4 ed., 2007.
[3] United States Department of Agriculture, Urban Hydrology for Small Watersheds (TR-55), 1986.

[4] Ethiopian Roads Authority, Bridge Design Manual – Part 1: Standards/Specifications for Bridge Design, 2013.
[5] NASA/METI/AIST & ASTER Science Team, Aster gdem version 3 dataset: Global digital elevation model of land areas on earth at a spatial resolution of 1 arc second, 2013. Accessed April 2, 2024.
[6] Food and Agriculture Organization of the United Nations, Land and Water Development Division, The digital soil map of the world (version 3.6), 2003.
[7] International Water Management Institute, Ethiopia wet seasonal rainfall, GIS Living Atlas, 2023.
[8] United States Geological Survey, Moderate resolution imaging spectroradiometer (modis) land cover type (mcd12q1) version 6.1: 2021 scenery, 2022. Accessed April 1, 2024.
[9] Land Processes Distributed Active Archive Center, Modis/terra land cover types yearly l3 global 0.05deg cmg (mod12c1), 2005.
[10] Ethiopian Roads Authority, Geometric Design Manual, 2013.
[11] T. Hengl, G. B. M. Heuvelink, B. Kempen, J. G. B. Leenaars, M. G. Walsh, K. D. Shepherd, A. Sila, R. A. MacMillan, J. Mendes de Jesus, L. Tamene, et al., Mapping soil properties of africa at 250 m resolution: Random forests significantly improve current predictions, 2015. doi:10.1371/journal.pone.0125814.
[12] Soil Science Division Staff, Soil Survey Manual, number 18 in USDA Handbook, U.S. Government Printing Office, Washington, D.C., 2017.